Control Of Small Two-Body Heaving Wave Energy Converters for Ocean Measurement Applications

Ossama Abdelkhalik[1] and Shangyan Zou[2]

Michigan Technological University
Mechanical Engineering -Engineering Mechanics Department
Houghton, MI, USA

Abstract

Buoys carrying scientific equipment usually need continuous power supply for the operation of these equipments. These buoys can be equipped with actuators and controlled to harvest power from the heaving motion of the buoy. A two-body wave energy converter can be designed such that the buoy heaves to harvest energy while the second (lower) body carries the science equipments. This paper presents a control approach for this type of two-body wave energy converter. This control approach is a multi resonant control that attempts to maximize the harvested energy from the buoy (upper body). In this model, the actuator is attached to both bodies. The lower body however is required to have minimal heave motion. The proposed multi resonant control utilizes measurements of the buoy position. The frequencies of the measured buoy position are estimated, along with the motion amplitudes of these frequencies, and used for feedback control. Estimation is carried out using two approaches; the first uses a linear Kalman filter while the second uses an extended Kalman filter. A new method for handling the motion and actuation limitations, suitable for the multi resonant control, is proposed. Various numerical simulation results are presented in the paper. Simulation results show that the linear Kalman filter estimation approach is more robust and computationally efficient compared to the extended Kalman filter.

Keywords: Wave Energy Conversion, Two-Body Heaving Wave Energy Converter, Multi Resonant Control, Kalman Filter

1. Introduction

Research on ocean wave energy converters (WECs) have been going since 1970s [1] covering several aspects including the hydrodynamics of interaction between a buoy and the wave [2, 3, 4], and including different concepts for ocean

[1]Associate Professor, Email: ooabdelk@mtu.edu, Tel. +1(906)487-3503
[2]PhD Candidate, Email: szou2@mtu.edu

Preprint submitted to Renewable Energy *May 17, 2018*

wave energy harvesting such as oscillating water column devices [5], overtopping converters [6] and the point absorbers [7, 8, 9]. In point absorbers, a buoy is controlled through actuators that act on the buoy against the seabed (single-body point absorber), or against a submerged larger mass that is not moving significantly (two-body point absorber). The single-body point absorber has been significantly studied over the past decades. Numerous controllers have been developed for the single-body point absorber such as those in references [10, 11, 12, 13, 14]. The two-body point absorber consists of two bodies: the upper body (buoy) and lower body. In fact the two-body point absorbers can be considered as a special category of the multi-body WECs, which are groups of closely spaced point absorbers, studied in several references such as [15, 16, 17]. This concept of two-body point absorber is investigated in this paper in more detail to explore the possibility of using this two-body WEC to generate enough power to supply scientific instruments mounted on the lower body of the two-body point absorber. The focus here is on the control strategy. A fundamental constraint in this problem is the maximum stroke of the actuator; the actuator connects the two bodies and both are moving. The lower body motion should be kept at minimum since it is a requirement for proper operation of the scientific equipments on the lower body. The linear analysis presented in this paper also enforces a small displacement constraint on the motion of the upper body.

There has been a significant amount of research on the two-body WECs in the literature. The hydrodynamics of the interaction between two cylinders is studied by [18] with infinite series of orthogonal functions. Reference [19] computes the radiation forces when the submerged cylinder has a larger radius than the floating one. The interaction between a cylinder at the top and a sphere at the bottom is studied in [20, 21]. References [22, 23, 24] present a detailed study for the hydrodynamic forces when the two-body system is composed of an outer hollow circular cylinder and an inner cylinder. Reference [25] studies the system response of a two-body system by means of the Reynolds-averaged Navier-stokes simulation. A dome-shaped buoy that reacts against a submerged spherical body is investigated in [26]. Reference [27] explores two independent oscillating bodies with a power take-off (PTO) unit attached to each one of them. Studying the relative motion of the two-body system is investigated in reference [28]. In fact reference [28] predicts the maximum power that can be harvested from the two-body system. Reference [29] compares two different systems; the first has the reaction mass out of the water while the second one assumes the reaction mass is submerged in the water. The results show that the system with a submerged reaction mass has a better performance. Recently, Reference [30] pointed out that the mass and viscous damping of the submerged body needs to be designed larger to achieve a better energy absorption of the two body heaving system. Reference [31] shows the system response and the energy absorption of a heaving two-cylinder WEC system. Reference [32] presents a latching phase control for the Interproject Service (IPS) buoy which is a two-body heaving system. The latching control is also studied in [33] for a two-body heaving system, and the performance of the controller is evaluated with real sea states. Reference [34] implements a PD controller and optimizes the controller gains using the Pontryagin Maximum Principle. The pseudo-spectrum method is also developed in [35] to control the motion of a self-reacting point absorber. A model predictive control is derived in [36] using the one-body equivalent model developed in [28].

Recently, a multi resonant control was developed for a single body point absorber, and is presented in references [37, 38]. The multi resonant control strategy implements a PD control to resonate the buoy motion with the incoming wave, at each frequency. The complex conjugate control (C3) criteria [1] are used in the multi resonant control to achieve resonance at each frequency. Yet, this multi resonant control is essentially a time-domain realization of the C3 controller. One advantage of the multi resonant control is elimination for the need of wave prediction; it is purely a feedback control. Yet, the the feedback signal (the buoy position signal) needs to be spectrally decomposed to obtain the motion amplitude at each frequency. This decomposition is carried out using a Fast Fourier Transform (FFT) approach in [37, 38].

This paper extends the multi resonant control for the case of a two-body WEC. Two-body WECs were recently proposed to generate power necessary for oceanic scientific missions [39]. A Kalman Filter is proposed to carry out the feedback signal decomposition instead of the FFT approach, and it is shown that the Kalman Filter has better performance and lower computational cost. Another contribution in this paper is a new concept for handling constraints on the WEC motion and actuation force. The original PDC3 approach is designed for the unconstraint case. This paper proposes a method for handling constraints suitable for the PDC3. This paper is organized as follows. Section 2 introduces the dynamic model of the two-body heaving system. Section 3 presents the development of the multi resonant control for the two-body system. Section 4 presents the signal processing part using the Kalman Filter. The simulation results, which show a comparison between the Extended Kalman Filter and the Linear Kalman Filter as well as a comparison between the unconstrained controller and the constrained controller, are presented in Section 5. Finally, the influence of different mooring stiffness is discussed in Section 6.

2. Dynamic Model

The proposed two-body heaving system in this paper is indicated in Fig. 1. The system consists of two bodies: a floating body and a submerged body (that may contain science sensors.) The two bodies are connected through a power take-off unit in between them. The heaving motion of the floating body is used to harvest energy by the power take-off unit. The submerged body is composed of two hemispheres; this structures has advantages in terms of the relative radiation damping between the two bodies as detailed in [39]. This submerged body of two hemispheres is adopted in this paper; yet the methods presented in this paper are applicable to any two-body heaving system. The Power take-off unit and the mooring are not shown in the figure, but they exist. The floating buoy is a cylinder, and the submerged body consists of two hemispheres that are rigidly connected. From now on, the upper and lower bodies will be denoted as body 1 and body 2, respectively.

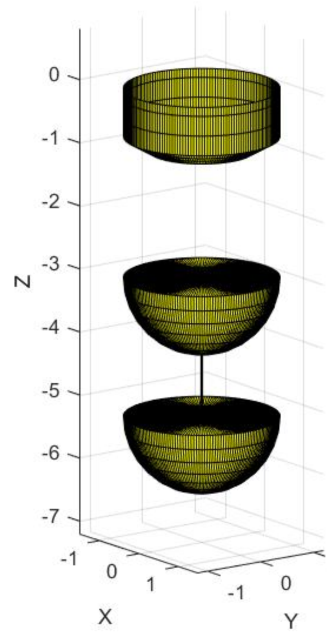

Figure 1: The two-body WEC system

The equations of motion of this two-body system in the case of a regular wave can be written as:

$$(m_1 + m_{a,11})\ddot{x}_1 + m_{a,12}\ddot{x}_2 + R_{11}\dot{x}_1 + R_{12}\dot{x}_2 + b_{v1}\dot{x}_1 + k_s x_1 = F_{e1} + u \quad (1)$$

$$(m_2 + m_{a,22})\ddot{x}_2 + m_{a,21}\ddot{x}_1 + R_{21}\dot{x}_1 + R_{22}\dot{x}_2 + b_{v2}\dot{x}_2 + k_m x_2 = F_{e2} - u \quad (2)$$

Where x_1 and x_2 represent the displacements of the first and second bodies, respectively, relative to their static equilibrium positions. The masses of the two bodies are m_1 and m_2. The $m_{a,ij}$ and R_{ij} are the added mass and radiation damping coefficient of the ith body due to the motion of the jth body, which are computed from the Boundary Element Software WAMIT [40]. The k_s is the hydrostatic stiffness of the first mass and k_m is the mooring stiffness of the second mass. The b_{v1} and b_{v2} are the viscous damping coefficients of body 1 and body 2, respectively. The control force (also called the Power take-off force) is generated by an actuator that is connected between the two bodies, and hence the control force u has the same magnitude in Equations (1) and (2), and with opposite directions. The F_{e1} and F_{e2} are the excitation forces on the first and the second bodies, respectively. As shown in Eq. (3), the excitation force is composed of the summation of several harmonics, that have different frequencies.

$$F_{e,i} = \sum_{n=1}^{N} \Re(\tilde{F}_{e,i}(\omega_n)\eta(\omega_n)e^{J(-\omega_n t+\phi_n)}), i = 1, 2 \tag{3}$$

where $\tilde{F}_{e,i}(\omega_n)$ represents the excitation force coefficient at the frequency ω_n, for the ith body, which is also obtained from WAMIT. The $\eta(\omega_n)$ is the frequency dependent wave elevation. The equation of motion can be written in a compact state space form as follows:

$$\mathbf{M}\ddot{\vec{x}} + \mathbf{B}\dot{\vec{x}} + \mathbf{K}\vec{x} = \vec{F}_e + \vec{F}_{rad} + \vec{u} \tag{4}$$

where the state vector $\vec{x} = [x_1, x_2]^T$. The excitation force vector $\vec{F}_e = [F_{e1}, F_{e2}]^T$, the radiation force vector $\vec{F}_{rad} = [F_{rad1}, F_{rad2}]^T$ and the control force vector $\vec{u} = [u, -u]^T$. The mass matrix is:

$$M = \begin{bmatrix} m_1 + m_{a,11} & m_{a,12} \\ m_{a,21} & m_2 + m_{a,22} \end{bmatrix} \tag{5}$$

The viscous damping matrix is:

$$B = \begin{bmatrix} b_{v1} & 0 \\ 0 & b_{v2} \end{bmatrix} \tag{6}$$

The stiffness $\mathbf{K}$ matrix is:

$$K = \begin{bmatrix} k_s & 0 \\ 0 & k_m \end{bmatrix} \tag{7}$$

The radiation force $\vec{F}_{rad}$ can be approximated by a state space model [41]:

$$\dot{\vec{x}}_r = A_r\vec{x}_r + B_r\dot{\vec{x}} \tag{8}$$

$$\vec{F}_{rad} = C_r\vec{x}_r \tag{9}$$

where A_r, B_r and C_r matrices are functions of the added masses and the radiation damping coefficients.

3. The Multi Resonant Control

The multi resonant control, which is also called the Proportional Derivative Complex Conjugate Controller (PDC3), uses a PD feedback control at each frequency to compute a control force at each frequency. The total feedback control is the summation of all the control forces at all frequencies. The details of the controller are presented in [42] for a single-body WEC. In this paper, the second mass is assumed to have a small motion. So the PDC3 controller is designed for the upper mass. At a frequency ω_i, the control force has the form:

$$u_i = -K_{p,i} x_{1,i} - K_{d,i} \dot{x}_{1,i} \tag{10}$$

where $x_{1,i}$ is the first body response at the ith frequency ω_i, that is:

$$\ddot{x}_{1,i} = -\frac{k_s}{m_1 + m_{a,11,i}} x_{1,i} - \frac{b_{v1} + R_{11,i}}{m_1 + m_{a,11,i}} \dot{x}_{1,i} + \frac{F_{e1,i} + u_i}{m_1 + m_{a,11,i}} \tag{11}$$

The $K_{p,i}$ and $K_{d,i}$ are the proportional and derivative gains of the controller respectively. To achieve the resonant condition, the $K_{p,i}$ and $K_{d,i}$ need to be designed as follows:

$$K_{p,i} = \omega_{ex}^2 (m_1 + m_{a,11,i}) - k_s \tag{12}$$

$$K_{d,i} = b_{v1} + R_{11,i} \tag{13}$$

As shown in Eq. (12) and (13), the concept of impedance matching (a C3 criterion) is used to design the PD gains. The system response x_1 is compounded from all frequencies; therefore N PD controllers can be designed as feedback signals.

$$u = \sum_{i=1}^{N} u_i \tag{14}$$

To compute the control in Eq. (10), the spectral decomposition of the first mass response x_1 and its derivative are needed. This spectral decomposition yields the amplitudes of position and velocity of the first body at each frequency. These amplitudes cannot be measured and hence they need to be estimated. For the sake of this estimation process, lets assume that the estimate of first body position signal $\hat{x}_1$ consists of N different harmonics:

$$\hat{x}_1 = \sum_{i=1}^{N} a_i \cos(\omega_i t) + b_i \sin(\omega_i t) \tag{15}$$

Hence:

$$\dot{\hat{x}}_1 = \sum_{i=1}^{N} -\omega_i a_i \sin(\omega_i t) + \omega_i b_i \cos(\omega_i t) \tag{16}$$

So based on Eqs. (10),(13), (15) and (16), Eq. (14) can be rewrite as:

$$u = -\sum_{i=1}^{N} K_{p,i}(a_i \cos(\omega_i t) + b_i \sin(\omega_i t)) - \sum_{i=1}^{N} (R_{11,i}(-\omega_i a_i \sin(\omega_i t) + \omega_i b_i \cos(\omega_i t))) - b_{v1}\dot{\hat{x}}_1 \tag{17}$$

where $[a_1, a_2, ... a_N]$, $[b_1, b_2, ... b_N]$, and $[\omega_1, \omega_2, ... \omega_N]$ are the unknown parameters to be estimated. Note that the b_{v1} is a frequency-independent constant, and hence it can be multiplied directly with the estimate of the velocity of the first body, as shown in Eq. (17).

The above PDC3 solves the unconstrained problem. There are usually constraints on the motion amplitude as well as limitations on the control force, in most realistic applications. To satisfy these constraints, the following concept is proposed. In the above unconstrained control, recall that N frequencies are selected and the control component at each frequency is designed so as to resonate the buoy motion with the wave at that frequency, according to the C3 criteria. These frequencies are those that have the largest N motion amplitudes; the value of N is usually selected so that most of the energy is captured. In the presence of motion and/or force constraints, it is possible to reduce the value of N such that the constraints are satisfied. Reducing the value of N implies resonating the buoy motion with the wave excitation force at fewer frequencies, which means reduced harvested energy. This reduction in the value of N, results in reduced control force and reduced motion amplitude, as detailed in Section 5. Hence, the process of handling constraints is to first compute the unconstrained PDC3, and if any of the constraints is violated then the number of frequencies is reduced to get a control force that satisfies all the constraints.

4. State Estimation

The Fast Fourier Transform (FFT) approach was the first attempt at estimating the amplitudes of motion as detailed in [37, 38]. Then a Least Squares Error Minimization approach was implemented in [42] for the same purpose. Both methods work on a time window to collect the data for signal processing. In this paper, the Kalman Filter, which is a recursive filter that does not need a time window, is implemented. It is demonstrated in this paper that the Kalman Filter not only accelerates the signal processing calculations but also can make the estimation more robust. Both a Linear Kalman Filter (LKF) and an Extended Kalman Filter (EKF) implementations are presented in this paper.

4.1. The Linear Kalman Filter

Consider Eqs.(15) and (16), if the frequencies are known then the position and velocity become linear functions of the a_i and b_i coefficients. In such case, LKF can be implemented. Hence we assume a vector of frequencies $\vec{\omega} = [\omega_1, \omega_2 \ldots \omega_N]^T$ to be known. Let us define the state vector of the Kalman Filter as $\hat{\mathbf{X}} = [\hat{a}_1, \hat{a}_2 \ldots \hat{a}_N, \hat{b}_1, \hat{b}_2 \ldots \hat{b}_N]^T$. The dynamics of the Kalman Filter can be written as:

$$\dot{\hat{\mathbf{X}}} = \mathbf{0} \qquad \text{and} \qquad \dot{P} = Q \tag{18}$$

where Q is the covariance matrix associated with the process noise, and P is the state estimate covariance matrix. The position measurement is represented as:

$$\tilde{y}_k = \sum_{i=1}^{N} (\hat{a}_i \cos(\omega_i t) + \hat{b}_i \sin(\omega_i t)) + v_k \tag{19}$$

where v_k is the measurement noise. The measurement in this case is the displacement of the first body, denoted as x_{1m}. This equation can be written in a more convenient form:

$$\tilde{y}_k = H_k \hat{\mathbf{X}}_k + v_k \tag{20}$$

where H is an $N \times 2$ matrix that include all the cosine and sine functions. Note that this H matrix can be computed off line since the frequency vector is assumed known. The Kalman gain at time step k is computed as:

$$K_k = P_k^- H_k^T [H_k P_k^- H_k^T + R_k]^{-1} \tag{21}$$

where R is the measurement noise covariance matrix. Finally, the process of the continuous-discrete LKF can be summarized as [43]:

(1) Propagate the current state and the covariance matrix using Eq. (18) to the next stage k, to get $\hat{\mathbf{X}}_k^-$ and P_k^-.

(2) Compute the Kalman Gain using Eq. (21).

(3) Update the state $\hat{\mathbf{X}}_k^-$ using:

$$\hat{\mathbf{X}}_k^+ = \hat{\mathbf{X}}_k^- + K_k [x_{1m,k} - H_k \hat{\mathbf{X}}_k^-] \tag{22}$$

(4) Update the state P_k^- using:

$$P_k^+ = [I - K_k H_k] P_k^- \tag{23}$$

(5) The current state becomes $\hat{\mathbf{X}}_k^+$ and P_k^+.

(6) Go to step (1)

To complete the implementation of the LKF, the $\hat{\mathbf{X}}_i$ and P_i need to be initialized when $i = 0$. Since all the hydrodynamic coefficients can be computed based on the shape of the buoy. Hence an initial guess $\hat{\mathbf{X}}_0$ can be computed as follows:

$$\hat{a}_i = \frac{\Re(\tilde{F}_{e1}(\omega_i))\eta_{max}/N}{\sqrt{(-(m_1 + m_{a,11,i})\omega_i^2 + k_s)^2 + (b_{v1} + R_{11,i})^2}}$$
$$\hat{b}_i = \frac{\Im(\tilde{F}_{e1}(\omega_i))\eta_{max}/N}{\sqrt{(-(m_1 + m_{a,11,i})\omega_i^2 + k_s)^2 + (b_{v1} + R_{11,i})^2}}$$
$$i = 1, 2, 3...N \tag{24}$$

where η_{max} is the maximum wave elevation which is assumed known. The $\vec{\omega}$ are selected to be evenly distributed within a certain range. The $\hat{\vec{a}}$, $\hat{\vec{b}}$ and $\vec{\omega}$ will be fed to the PDC3 controller.

4.2. The Extended Kalman Filter

If the frequency vector in the model described in Section 3 is unknown, then it needs to be estimated. Adding $\vec{\omega}$ to the state vector renders the system nonlinear and hence an extended Kalman filter is needed. So the state vector in this case becomes:

$$\hat{\mathbf{X}} = [\hat{x}_1,\, \hat{\dot{x}}_1,\, \hat{\vec{x}}_{r11},\, \hat{\vec{A}},\, \hat{\vec{B}},\, \hat{\vec{a}},\, \hat{\vec{b}},\, \hat{\vec{\omega}}] \tag{25}$$

where $\hat{\vec{A}}$ and $\hat{\vec{B}}$ are the estimates for the coefficients in Eq. (26) which represents the series expansion approximation for the excitation force on the first body:

$$\hat{F}_{e1} = \sum_{i=1}^{N} A_i \cos(\omega_i t) + B_i \sin(\omega_i t) \tag{26}$$

The dynamic equations used in the EKF are listed below:

$$\begin{aligned}
\hat{\ddot{x}}_1 &= \frac{1}{M_{11}}(\hat{F}_{e1} + u - C_{r11}\hat{\vec{x}}_{r11} - b_{v1}\hat{\dot{x}}_1 - k_s\hat{x}_1) \\
\hat{\dot{x}}_{r11} &= A_{r11}\hat{\vec{x}}_{r11} + B_{r11}\hat{\dot{z}}_1 \\
\hat{\dot{\vec{A}}} = \hat{\dot{\vec{B}}} &= \hat{\dot{\vec{a}}} = \hat{\dot{\vec{b}}} = \hat{\dot{\vec{\omega}}} = \mathbf{0}
\end{aligned} \tag{27}$$

where $M_{11} = (m_1 + m_{a,11})$ is the summation of the first rigid body mass and the added mass due to the first body radiation waves. The $\hat{x}_1$ is the estimation for the displacement of the first mass, $\hat{\vec{x}}_{r11}$ represents the estimation for the radiation states associated with the radiation force on the first mass due to the radiation waves generated by the first mass. The A_{r11}, B_{r11} and C_{r11} can be obtained from WAMIT. Note that in this EKF dynamic model we neglected the effect of radiation force from the radiated waves generated by the second body on the first body for couple of reasons. First, it is assumed that the motion of the second body is small and hence its impact is small. Second, this model is used only inside the EKF to propagate the first body motion. The propagated states get updated at each time step using the measurements, and hence a small error in the propagation step might be acceptable for the sake of having faster and computationally efficient estimation. To propagate the EKF, we need to compute the Jacobian matrix F which includes the partial derivatives of each of the dynamic equations (27) with respect to each of the states. The matrix F is then:

$$M_{11}F = \begin{bmatrix} 0 & 1 & \mathbf{0} & \mathbf{0} & \mathbf{0} & \mathbf{0} & \mathbf{0} & \mathbf{0} \\ -k_s & -b_{v1} & -C_{r11} & \frac{\partial f_2}{\partial \hat{\vec{A}}} & \frac{\partial f_2}{\partial \hat{\vec{B}}} & \mathbf{0} & \mathbf{0} & \frac{\partial f_2}{\partial \hat{\vec{\omega}}} \\ \mathbf{0} & M_{11}B_{r11} & M_{11}A_{r11} & \mathbf{0} & \mathbf{0} & \mathbf{0} & \mathbf{0} & \mathbf{0} \\ \mathbf{0} & \mathbf{0} & \mathbf{0} & \mathbf{0} & \mathbf{0} & \mathbf{0} & \mathbf{0} & \mathbf{0} \\ \mathbf{0} & \mathbf{0} & \mathbf{0} & \mathbf{0} & \mathbf{0} & \mathbf{0} & \mathbf{0} & \mathbf{0} \\ \mathbf{0} & \mathbf{0} & \mathbf{0} & \mathbf{0} & \mathbf{0} & \mathbf{0} & \mathbf{0} & \mathbf{0} \\ \mathbf{0} & \mathbf{0} & \mathbf{0} & \mathbf{0} & \mathbf{0} & \mathbf{0} & \mathbf{0} & \mathbf{0} \\ \mathbf{0} & \mathbf{0} & \mathbf{0} & \mathbf{0} & \mathbf{0} & \mathbf{0} & \mathbf{0} & \mathbf{0} \end{bmatrix} \tag{28}$$

where

$$\frac{\partial f_2}{\partial \hat{\vec{A}}} = \cos(\hat{\vec{\omega}}t) \tag{29}$$

$$\frac{\partial f_2}{\partial \hat{\vec{B}}} = \sin(\hat{\vec{\omega}}t) \tag{30}$$

$$\frac{\partial f_2}{\partial \hat{\vec{\omega}}} = -\hat{\vec{\omega}} \cdot \hat{\vec{A}} \cdot \sin(\hat{\vec{\omega}}t) + \hat{\vec{\omega}} \cdot \hat{\vec{B}} \cdot \cos(\hat{\vec{\omega}}t) \tag{31}$$

The Jacobian matrix F is used to propagate the covariance matrix:

$$\dot{P} = FP + PF^T + Q \tag{32}$$

The measurement at a time step k is:

$$\begin{aligned} \tilde{y}_k &= h(\hat{\mathbf{X}}_k) + v_k \\ &= \left[\sum_{i=1}^{N} \hat{a}_i \cos(\hat{\omega}_i t) + \hat{b}_i \sin(\hat{\omega}_i t) \right] + v_k \end{aligned} \tag{33}$$

where v_k is the measurement noise. So the Jacobian matrix of the output H can be computed as:

$$H = \begin{bmatrix} 1 & 0 & \mathbf{0} & \mathbf{0} & \mathbf{0} & \mathbf{0} & \mathbf{0} & \mathbf{0} \\ 0 & 0 & \mathbf{0} & \mathbf{0} & \mathbf{0} & \cos(\hat{\vec{\omega}}t) & \sin(\hat{\vec{\omega}}t) & \frac{\partial h_2}{\hat{\vec{\omega}}} \end{bmatrix} \tag{34}$$

where

$$\frac{\partial h_2}{\hat{\vec{\omega}}} = -\hat{\vec{\omega}} \cdot \hat{\vec{a}} \cdot \sin(\hat{\vec{\omega}} t) + \hat{\vec{\omega}} \cdot \hat{\vec{b}} \cdot \cos(\hat{\vec{\omega}} t) \tag{35}$$

The Kalman gain of the EKF can be computed as:

$$K_k = P_k^- H_k^T(\hat{\mathbf{X}}_k^-)[H_k(\hat{\mathbf{X}}_k^-) P_k^- H_k^T(\hat{\mathbf{X}}_k^-) + R_k]^{-1} \tag{36}$$

The process of the continuous-discrete EKF can be summerized as:

(1) Propagate the current state and the covariance matrix with Eq. (27) and (32) to the next stage k to get $\hat{\mathbf{X}}_k^-$ and P_k^-.

(2) Compute the Kalman Gain using Eq. (36).

(3) Update the state $\hat{\mathbf{X}}_k^-$ using:

$$\hat{\mathbf{X}}_k^+ = \hat{\mathbf{X}}_k^- + K_k \left[[x_{1m,k},\, x_{1m,k}]^T - h(\hat{\mathbf{X}}_k^-) \right] \tag{37}$$

(4) Update the state P_k^- using:

$$P_k^+ = [I - K_k H_k(\hat{\mathbf{X}}_k^-)] P_k^- \tag{38}$$

(5) The current state becomes $\hat{\mathbf{X}}_k^+$ and P_k^+.

(6) Go to step (1)

5. Simulation results

The first mass used in the simulation has a radius of 1.2 m and a draft of 1 m. The second mass has a radius of 1.2 m for both hemispheres. The rigid body mass of the first body is 4637 kg, and of the second body is 7419.2 kg. Matlab$^{\text{TM}}$ has been used for all the simulations. The PC used for simulations has an Intel Core$^{\text{TM}}$ i5 CPU at $3.3GHz$ and with $8.0GB$ memory. The control update rate utilized in the simulation is 0.01s.

5.1. Comparison between LKF and EKF

The wave used in this section has a Bretschneider wave spectrum that is realized using 300 frequencies. The significant height of the wave is 0.2 m, and the peak period varies from 6 s to 12 s. The mooring stiffness of the second mass is 3.63×10^6 N/m. The PDC3 controller with EKF uses 5 PD controllers. The LKF, however, uses 11 PD controllers at fixed 11 frequencies. The values of the vector of the frequencies are equally spaced and are shown below:

$$\begin{aligned}\vec{\omega} = [&0.005,\, 0.143,\, 0.2811,\, 0.4191,\, 0.5571,\, 0.6952,\\ &0.8332,\, 0.9712,\, 1.1092,\, 1.2473,\, 1.3853]^T (rad/s)\end{aligned} \tag{39}$$

The average extracted power of the two-body system for each of the LKF and the EKF at different peak periods are shown in Fig. 2. The performance of the LKF is clearly more robust compared to the EKF due to the higher estimation accuracy obtained by the LKF. Regarding the computational cost, the significant part of the computational cost is in the estimation algorithm. The EKF needs 0.0048 s for estimation in each time step. The LKF needs 0.0021 s for estimation in each time step. Hence, the LKF is about twice as fast compared to the EKF. Therefore, the rest of this paper will show only results obtained using the LKF.

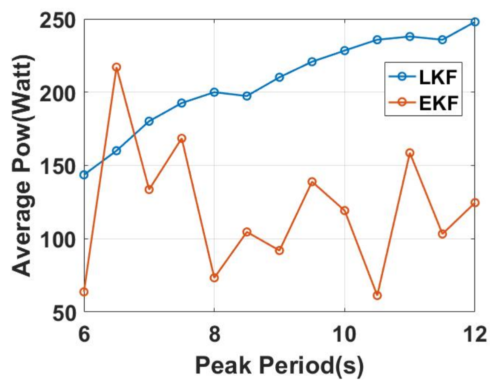

Figure 2: The average extracted power for a range of peak periods using both LKF and EKF

5.2. The Unconstrained Problem

The detailed results for the performance of the unconstrained PDC3 controller, using the LKF for estimation, is presented in this section. The wave used in this section has a significant height of 0.2 m, and has a peak period of 9 s. The mooring stiffness of the second mass is 3.63×10^6 N/m. The multi resonant controller has 11 PD feedback controllers. The distribution of the frequencies is the same as in Eq. (39). Figures 3 and 4 show the harvested power and energy from each of the two bodies. It can be seen from Figs. 3 and 4 that the average extracted power is 210 W within 500 s. The motion of the buoy is shown in Fig. 5 which indicates a maximum displacement of 1.6 m of body 1. Fig. 6 shows the displacement estimation which is clearly close to the true displacement. The maximum relative motion is also around 1.6 m due to the small motion of body 2. The control force is plotted in Fig. 7, the maximum control force is below 7×10^4 N.

5.3. The Constrained Problem

There are few constraints that need to be accounted for in a realistic implementation of the proposed PDC3 control on the two-body WEC. In this case study, it is assumed that the maximum displacement for the first mass is 0.9 m,

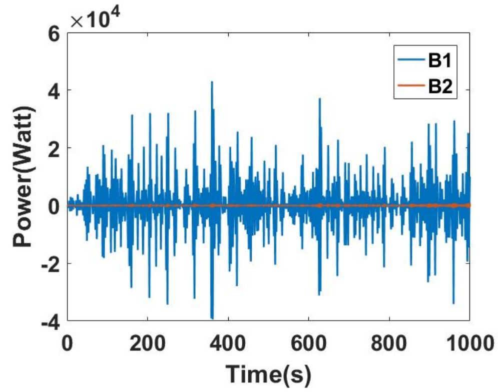

Figure 3: The extracted power for each of body 1 and body 2

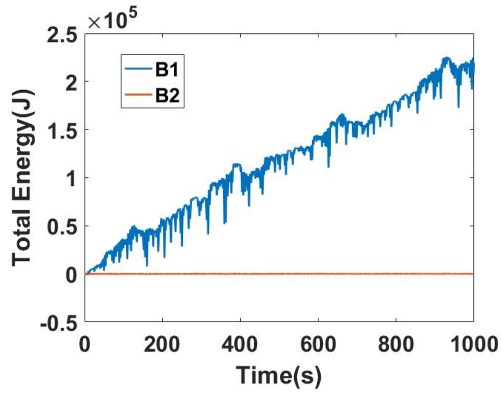

Figure 4: The extracted energy for each of body 1 and body 2

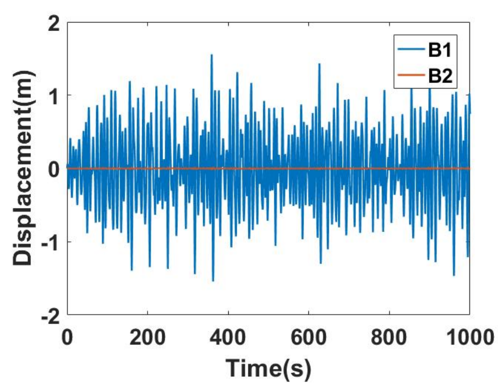

Figure 5: The displacement of each of body 1 and body 2

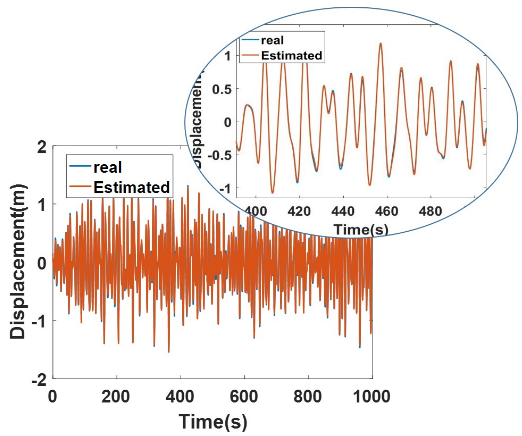

Figure 6: The real vs. the estimated displacement of body 1

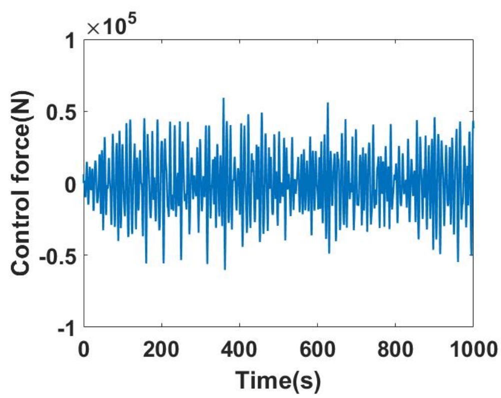

Figure 7: The control force on body 1

and the maximum relative motion is 1.5 m. The control force is limited below 7000 N. The wave used in this section has a significant height of 0.3 m and a peak period of 9 s. The mooring stiffness is 3.63×10^6 N/m. To satisfy the constraint for the control force, the number of frequencies is reduced to $N = 4$. These frequencies are $\vec{\omega} = [0.005, 0.4651, 0.9252, 1.3853]$ rad/s.

Figure 8 shows the energy extracted in 1000 s by each of body 1 and body 2. The harvested energy by body 1 is 1.421×10^5 J and the harvested energy by by body 2 is 301.9 J. This is equivalent to an average power of 140 W. Fig. 9 shows that the maximum displacement of body 1 is around 0.5 m; the displacement is not plotted but it is very small and negligible due to mooring. The estimation accuracy of the displacement is shown in Fig. 9 where both the estimated and true displacements are presented. Since the motion of body 2 is very small, the relative motion then has a maximum magnitude of around 0.5 m. Using only 4 frequencies in computing the control reduces the control level significantly.

When it is still higher than the control constraint, the control force is forced to have the maximum control level as shown in Fig. 10.

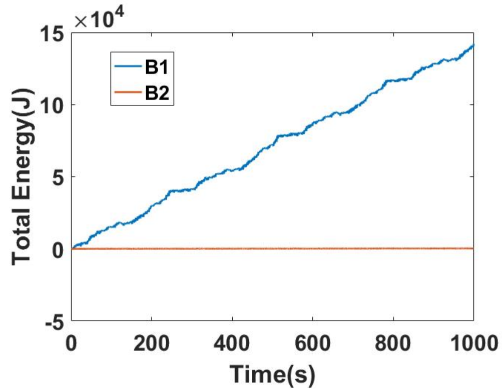

Figure 8: The extracted energy of body 1 and body 2

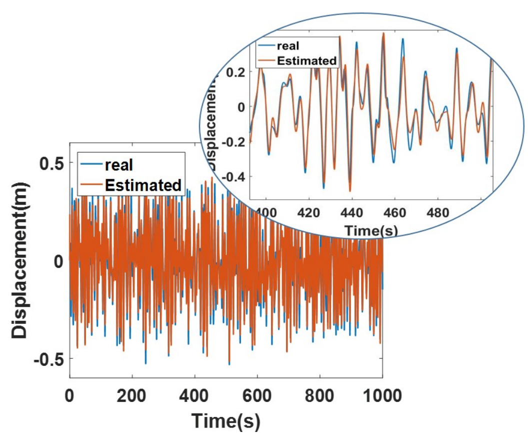

Figure 9: The real displacement of body 1 and the estimated displacement

6. Discussion

In this paper, the PDC3 controller is presented to control the motion of the two-body system shown in Fig. 1. After comparing the performance of the LKF and EKF, the LKF is selected to estimate the system states. It is noted here that the LKF does not require any wave information. Moreover, the computational cost is significantly saved by the LKF because of the simplicity of the dynamics of LKF. In previous work, the parameters estimation was conducted using either FFT [37, 38] or a Least Squares Error minimization approach [42]. A large time window was needed in both methods to collect sufficient data for

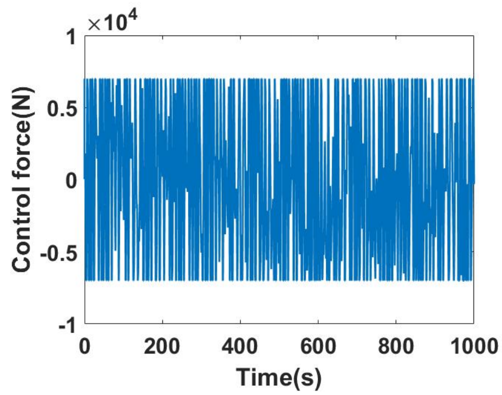

Figure 10: The control force

signal processing, and the optimal window size also needed careful selection. The PDC3 control was sensitive to the accuracy of the estimated states in both methods. Nevertheless, the LKF overcomes these issues. No window is needed in this recursive LKF. Also there is a robust energy extraction, while the computational time is improved significantly.

It is assumed in this paper that the second body has a small motion, and a large mooring stiffness (3.63×10^6 N/m) is assumed for the second body in the results presented in Section 5. Here, the performance of the system is compared for several different mooring stiffness values. The investigated values of the mooring stiffness are $K = [10, 1000, 5 \times 10^4, 6 \times 10^5, 3.63 \times 10^6]$ N/m. Fig. 11 shows the variation of the average power harvested by body 1 as well as the total power harvested by the two bodies versus the mooring stiffness. Also Fig. 12 shows the variation of the relative displacement between the two masses versus the mooring stiffness. As can be seen in both figures, when the mooring stiffness is below 5×10^4 N/m ($\log(5 \times 10^4) = 10.8198$), the relative displacement between the two bodies is significantly high. The average absorbed power of the first body is about the same everywhere (about 145 W) in this range, while the second body moves and affects the harvested power. The motion of the second body is undesirable and hence this range of mooring stiffness values is not suitable. On the other hand, when the mooring stiffness is greater than 3.63×10^6 N/m ($\log(3.63 \times 10^6) = 15.1047$), the second mass will have very small motion and hence a minimum impact on the harvested energy by the system.

7. Conclusion

This paper presents a multi resonant controller for a two-body heaving system, in which the lower body is required to have minimal motion while harvested energy from the upper body is maximized. The concept of impedance matching

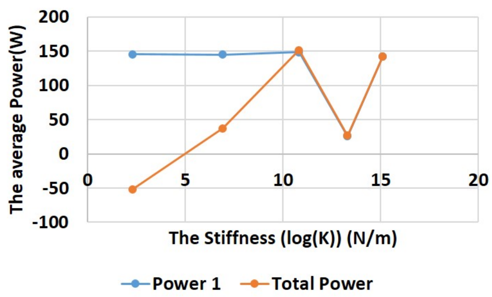

Figure 11: The power harvested by body 1 (Power 1) and the total harvested power by the two bodies for different mooring stiffness values

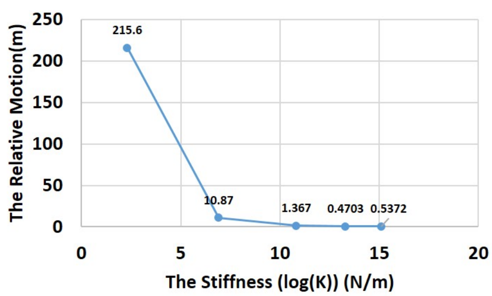

Figure 12: The maximum relative motion for different mooring stiffness values

is utilized in this multi resonant control and is realized using multiple PD control designs at multiple frequencies, in the feedback signal. This approach is a feedback approach that does not require wave prediction. Rather the spectral decomposition of the buoy motion amplitude at different frequencies is estimated. It is shown in this paper that a linear Kalman filter (LKF) can be used to estimate these amplitudes in a computationally efficient and more robust way, compared to fast Fourier transform, least square error methods, and an extended Kalman filter (EKF). This paper also presents a simple method for handling motion and control constraints when the PDC3 approach is implemented for control. High mooring stiffness is needed for the lower body when designing this type of control, due to the requirement of small motion of the second body. simulation results in this paper demonstrates the possibility of maintaining small displacements for the second body while harvesting energy from the first body. While the analysis conducted in this paper focuses on a specific two-body WEC, the methods presented are applicable to any type of two-body heaving system.

Acknowledgement

This material is based upon work supported by the National Science Foundation under Grant Number 1635362. Dr. Rush Robinett suggested the use of the multi resonant control in this application.

References

[1] J. Falnes, A review of wave-energy extraction, Marine Structures 20 (4) (2007) 185–201.

[2] C. C. Mei, Power extraction from water waves, Journal of Ship Research 20 (1976) 63–66.

[3] K. Budal, Theory for absorbtion of wave power by a system of interacting bodies, Journal of Ship Research 21 (1977) 248–253.

[4] J.N.Newman, The interaction of stationary vessels with regular waves, in: Proceeding 11th symposium, Naval hydrodynamics, London, 1976. doi:10.1017/S0022112076001109.
URL http://journals.cambridge.org/article_S0022112076001109

[5] A. F. Falcão, J. C. Henriques, Oscillating-water-column wave energy converters and air turbines: A review, Renewable Energy 85 (2016) 1391–1424.

[6] B. Drew, A. Plummer, M. N. Sahinkaya, A review of wave energy converter technology, Proceedings of the Institution of Mechanical Engineers, Part A: Journal of Power and Energy 223 (8) (2009) 887–902.

[7] J. Ringwood, G. Bacelli, F. Fusco, Energy-maximizing control of wave-energy converters: The development of control system technology to optimize their operation, Control Systems, IEEE 34 (5) (2014) 30–55. doi:10.1109/MCS.2014.2333253.

[8] F. Fusco, J. Ringwood, Hierarchical robust control of oscillating wave energy converters with uncertain dynamics, Sustainable Energy, IEEE Transactions on 5 (3) (2014) 958–966. doi:10.1109/TSTE.2014.2313479.

[9] J. Scruggs, S. Lattanzio, A. Taflanidis, I. Cassidy, Optimal causal control of a wave energy converter in a random sea, Applied Ocean Research 42 (2013) 1 – 15. doi:http://dx.doi.org/10.1016/j.apor.2013.03.004.
URL http://www.sciencedirect.com/science/article/pii/S0141118713000205

[10] G. Li, M. R. Belmont, Model predictive control of sea wave energy converters part i: A convex approach for the case of a single device, Renewable Energy 69 (0) (2014) 453 – 463. doi:http://dx.doi.org/10.1016/j.renene.2014.03.070.
URL http://www.sciencedirect.com/science/article/pii/S0960148114002456

[11] A. Babarit, A. H. Clément, Optimal latching control of a wave energy device in regular and irregular waves, Applied Ocean Research 28 (2) (2006) 77–91.

[12] E. Abraham, E. C. Kerrigan, Optimal active control and optimization of a wave energy converter, IEEE Transactions on Sustainable Energy 4 (2) (2013) 324–332.

[13] G. Bacelli, J. Ringwood, Numerical optimal control of wave energy converters, Sustainable Energy, IEEE Transactions on 6 (2) (2015) 294–302. doi:10.1109/TSTE.2014.2371536.

[14] S. Zou, O. Abdelkhalik, R. Robinett, G. Bacelli, D. Wilson, Optimal control of wave energy converters, Renewable Energy 103 (2017) 217 – 225. doi:http://dx.doi.org/10.1016/j.renene.2016.11.036.
URL http://www.sciencedirect.com/science/article/pii/S0960148116310059

[15] F. F. Flavià, A. Babarit, A. Clément, On the numerical modeling and optimization of a bottom-referenced heave-buoy array of wave energy converters, International Journal of Marine Energy.

[16] G. Barcelli, J. Ringwood, Constrained control of arrays of wave energy devices., International Journal of Marine Energy 3 (2013) 53–69.

[17] B. F. M. Child, On the configuration of arrays of floating wave energy converters.

[18] Y. Zheng, Y. Shen, Y. You, B. Wu, L. Rong, Hydrodynamic properties of two vertical truncated cylinders in waves, Ocean Engineering 32 (3) (2005) 241–271.

[19] B. Wu, Y. Zheng, Y. You, D. Jie, Y. Chen, On diffraction and radiation problem for two cylinders in water of finite depth, Ocean engineering 33 (5) (2006) 679–704.

[20] J. Engström, M. Eriksson, J. Isberg, M. Leijon, Wave energy converter with enhanced amplitude response at frequencies coinciding with swedish west coast sea states by use of a supplementary submerged body, Journal of Applied Physics 106 (6) (2009) 064512.

[21] J. Engström, V. Kurupath, J. Isberg, M. Leijon, A resonant two body system for a point absorbing wave energy converter with direct-driven linear generator, Journal of applied physics 110 (12) (2011) 124904.

[22] F. P. Chau, R. W. Yeung, Inertia and damping of heaving compound cylinders, in: Abstract for The 25th International Workshop on Water Waves and Floating Bodies, Harbin, China, 2010, pp. 1–4.

[23] C. Cochet, R. W. Yeung, Two-component axisymmetricwave-energy absorber-analysis of dynamics and geometric proportions, in: The 27th International Workshop on Water Waves and Floating Bodies, Copenhagen, Denmark, Citeseer, 2012.

[24] J. R. Kim, Y. H. Bae, I. H. Cho, et al., Relative heave motion responses of a floating dual-buoy wave energy converter in waves, in: The Twenty-fifth International Ocean and Polar Engineering Conference, International Society of Offshore and Polar Engineers, 2015.

[25] Y.-H. Yu, Y. Li, Reynolds-averaged navier–stokes simulation of the heave performance of a two-body floating-point absorber wave energy system, Computers & Fluids 73 (2013) 104–114.

[26] T. Whittaker, A. Wells, Experiences with a hydropneumatic wave power device, in: International Symposium on Wave and Tidal Energy, Vol. 1, 1978, pp. B4–57.

[27] M. Srokosz, D. Evans, A theory for wave-power absorption by two independently oscillating bodies, Journal of Fluid Mechanics 90 (02) (1979) 337–362.

[28] J. Falnes, Wave-energy conversion through relative motion between two single-mode oscillating bodies, Journal of Offshore Mechanics and Arctic Engineering 121 (1) (1999) 32–38.

[29] U. A. Korde, Systems of reactively loaded coupled oscillating bodies in wave energy conversion, Applied ocean research 25 (2) (2003) 79–91.

[30] C. Liang, L. Zuo, On the dynamics and design of a two-body wave energy converter, Renewable Energy 101 (2017) 265–274.

[31] B. Wu, X. Wang, X. Diao, W. Peng, Y. Zhang, Response and conversion efficiency of two degrees of freedom wave energy device, Ocean Engineering 76 (2014) 10–20.

[32] F. d. O. António, P. A. Justino, J. C. Henriques, J. M. André, Reactive versus latching phase control of a two-body heaving wave energy converter, in: Control Conference (ECC), 2009 European, IEEE, 2009, pp. 3731–3736.

[33] J. Henriques, M. Lopes, R. Gomes, L. Gato, A. Falcao, On the annual wave energy absorption by two-body heaving wecs with latching control, Renewable Energy 45 (2012) 31–40.

[34] J. J. Cândido, P. A. Justino, Modelling, control and pontryagin maximum principle for a two-body wave energy device, Renewable Energy 36 (5) (2011) 1545–1557.

[35] G. Bacelli, J. V. Ringwood, J.-C. Gilloteaux, A control system for a self-reacting point absorber wave energy converter subject to constraints, IFAC Proceedings Volumes 44 (1) (2011) 11387–11392.

[36] S. Olaya, J.-M. Bourgeot, M. Benbouzid, Optimal control for a self-reacting point absorber: A one-body equivalent model approach, in: Power Electronics and Application Conference and Exposition (PEAC), 2014 International, IEEE, 2014, pp. 332–337.

[37] J. Song, O. Abdelkhalik, R. Robinett, G. Bacelli, D. Wilson, U. Korde, Multi-resonant feedback control of heave wave energy converters, Ocean Engineering 127 (2016) 269 – 278. doi:http://dx.doi.org/10.1016/j.oceaneng.2016.09.046.
URL http://www.sciencedirect.com/science/article/pii/S0029801816304346

[38] O. Abdelkhalik, J. Song, R. Robinett, G. Bacelli, D. Wilson, U. Korde, Feedback control of wave energy converters, in: Asian Wave and Tidal Energy Conference (AWTEC 2016), Marina Bay Sands, Singabore, 2016, pp. 258–261.

[39] U. A. Korde, J. Song, R. D. Robinett, O. O. Abdelkhalik, Hydrodynamic considerations in near-optimal control of a small wave energy converter for ocean measurement applications, Marine Technology Society Journal 51 (6) (2017) 44–57. doi:doi:10.4031/MTSJ.51.6.5.
URL http://www.ingentaconnect.com/content/mts/mtsj/2017/00000051/00000006/art00006

[40] C. Lee, WAMIT Theory Manual, Report (Massachusetts Institute of Technology. Department of Ocean Engineering), Massachusetts Institute of Technology, Department of Ocean Engineering, 1995.
URL http://books.google.com/books?id=fWKGHAAACAAJ

[41] T. Pérez, T. I. Fossen, Time-vs. frequency-domain identification of parametric radiation force models for marine structures at zero speed, Modeling, Identification and Control 29 (1) (2008) 1–19.

[42] O. Abdelkhalik, S. Zou, R. Robinett, G. Bacelli, D. Wilson, R. Coe, U. A. Korde, Multi resonant feedback control of three-degree-of-freedom wave energy converters, IEEE Transactions on Sustainable Energy 8 (4) (2017) 1518–1527. doi:10.1109/TSTE.2017.2692647.

[43] J. L. Crassidis, J. L. Junkins, Optimal Estimation of Dynamic Systems, CHAPMAN&HALL/CRC, 2004.